Comp. Meth. Civil Eng. 2010, Vol. 1 No. 1 pp. 1-13

CMCE
Computational Methods in Civil Engineering

Element free Galerkin method for crack analysis of orthotropic plates

S.Sh. Ghorashi[a], S.R. Sabbagh-Yazdi[a,*], S. Mohammadi[b]

[a]*Department of Civil Engineering, KNToosi University of Technology, Tehran, Iran*
[b]*School of Civil Engineering, University of Tehran, Tehran, Iran*

Received 7 September 2010, accepted in revised form 20 December 2010

Abstract

A new approach for analyzing cracked problems in 2D orthotropic materials using the well-known element free Galerkin method and orthotropic enrichment functions is proposed. The element free Galerkin method is a meshfree method which enables discontinuous problems to be modeled efficiently. In this study, element free Galerkin is extrinsically enriched by the recently developed crack-tip orthotropic enrichment functions. Also, a suitable way is applied to select support domains near a crack so that the discontinuity can be modeled without the Heaviside enrichment function. Crack-tip enrichment functions span the possible displacement space that may occur in the analytical solution. For evaluating the mixed-mode stress intensity factors, the interaction integral is applied. Some numerical examples are simulated to investigate the efficacy of the new approach by comparing with other numerical or (semi-) analytical methods.

Keywords: Orthotropic material; Element free Galerkin method; Enrichment functions; Interaction integral; Stress intensity factors.

1. Introduction

Since the stiffness and strength per unit weight of orthotropic materials such as composites are higher than other conventional engineering materials in many cases, applications of these kinds of materials have been widely increased in recent decades. Considering their strength, they are applied in thin shell forms while crack initiation is probable to take place in them. As a result, analysis, modeling and investigation of fracture behavior of such materials have turned into a growing research subject.

Some analytical investigations have been performed on the fracture behavior of composite materials such as the pioneering one by Muskelishvili [1], Sih et al. [2] and more recently Nobile and Carloni [3].

The analytical solution is not applicable to all problems; in particular to complicated engineering cases, whereas, the numerical methods are the best available approaches for

* Corresponding author.
E-mail address: syazdi@kntu.ac.ir (S.R. Sabbagh-Yazdi)

studying such general problems. There are many numerical methods applied for modeling cracks in mechanical problems such as the Boundary Element Method (BEM), the Finite Difference Method (FDM), the Finite Volume Method (FVM), the Finite Element Method (FEM), the eXtended Finite Element Method (XFEM) and Meshless Methods (MMs) such as the Element Free Galerkin (EFG) method [4]. One of the main drawbacks of FEM is that elements associated with a crack must conform to crack faces. Furthermore, remeshing techniques are required to follow crack propagation patterns. Some drawbacks of FEM have been modified in XFEM but it is still necessary to introduce a mesh of elements at the beginning of modeling. Due to mesh-based interpolation, distorted or low quality meshes lead to higher errors, and necessitate remeshing, a time and human labour consuming task, which is not guaranteed to be feasible in a limited time for complex three-dimensional geometries. MMs were born with the objective of eliminating part of the difficulties associated with reliance on a mesh to construct the approximation. In MMs, the approximation is built from nodes only. Mainly they are more convenient for analysis of discontinuous problems. The element free Galerkin method [4] was developed in 1994 and was one of the first and famous MMs based on a global weak form.

On the other hand, in XFEM [5], the finite element approximation in the vicinity of the crack is enriched with appropriate enrichment functions extracted from the analytical analysis near a crack-tip. Two dimensional discontinuous problems in orthotropic materials have been analyzed by XFEM recently [6, 7, 8]. They developed three different sets of enrichment functions for various types of composites. It is, therefore, a feasible idea to use enrichment functions of XFEM in EFG for increasing the accuracy of analysis near crack-tip.

In this paper, the element free Galerkin method is extended to orthotropic materials by modification of the weight functions and adopting the orthotropic enrichment functions proposed by Asadpoure et al. [8]. In order to verify the formulation and to investigate the robustness of the proposed method, stress intensity factors (SIFs) for cracked media are obtained by the method proposed by Kim and Paulino [9] and compared with other numerical or (semi-) analytical methods.

2. Fracture mechanics in orthotropic media

The stress–strain law in an arbitrary linear elastic material can be written as

$$\boldsymbol{\varepsilon} = \mathbf{c}\boldsymbol{\sigma} \tag{1}$$

where $\boldsymbol{\varepsilon}$ and $\boldsymbol{\sigma}$ are strain and stress vectors, respectively, and $\mathbf{c}$ is the compliance matrix

$$\mathbf{c}^{3D} = \begin{bmatrix} \frac{1}{E_1} & -\frac{\nu_{21}}{E_2} & -\frac{\nu_{31}}{E_3} & 0 & 0 & 0 \\ -\frac{\nu_{12}}{E_1} & \frac{1}{E_2} & -\frac{\nu_{32}}{E_3} & 0 & 0 & 0 \\ -\frac{\nu_{13}}{E_1} & -\frac{\nu_{23}}{E_2} & \frac{1}{E_3} & 0 & 0 & 0 \\ 0 & 0 & 0 & \frac{1}{G_{23}} & 0 & 0 \\ 0 & 0 & 0 & 0 & \frac{1}{G_{13}} & 0 \\ 0 & 0 & 0 & 0 & 0 & \frac{1}{G_{12}} \end{bmatrix} \tag{2}$$

which E, ν and G are Young's modulus, Poisson's ratio and shear modulus, respectively. For a plane stress case the compliance matrix is reduced to the following form:

$$\mathbf{c}^{2D}=\begin{bmatrix} \frac{1}{E_1} & -\frac{\nu_{12}}{E_1} & 0 \\ -\frac{\nu_{12}}{E_1} & \frac{1}{E_2} & 0 \\ 0 & 0 & \frac{1}{G_{12}} \end{bmatrix} \tag{3}$$

and for a plane strain state

$$c_{ij}^{2D}=c_{ij}^{3D}-\frac{c_{i3}^{3D}.c_{j3}^{3D}}{c_{33}^{3D}} \quad i,j=1,2,6 \tag{4}$$

Now assume an anisotropic body subjected to arbitrary forces with general boundary conditions and a crack. Global Cartesian co-ordinate (X_1,X_2), local Cartesian co-ordinate (x,y) and local polar co-ordinate (r,θ), defined on the crack-tip, are illustrated in Figure 1. A fourth-order partial differential equation with the following characteristic equation can be obtained using equilibrium and compatibility conditions [10]

$$c_{11}s^4-2c_{16}s^3+\left(2c_{12}+c_{66}\right)s^2-2c_{26}s+c_{22}=0 \tag{5}$$

where c_{ij} $(i,j=1,2,6)$ are the components of $\mathbf{c}^{2D}$.

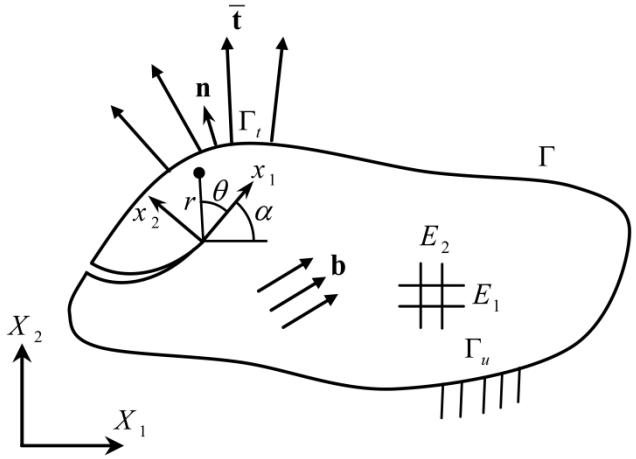

Figure 1. An arbitrary cracked orthotropic body subjected to body force $\mathbf{b}$ and traction $\bar{\mathbf{t}}$.

According to Lekhnitskii [10], the roots of equation (5) are always complex or purely imaginary ($s_k=s_{kx}+is_{ky}$, $k=1,2$) and occur in conjugate pairs as s_1, $\bar{s}_1$ and s_2, $\bar{s}_2$. The two-dimensional displacement and stress fields in the vicinity of the crack-tip have been derived as [2]

- Mode I

$$u^I=K_I\sqrt{\frac{2r}{\pi}}\,\mathrm{Re}\left[\frac{1}{s_1-s_2}\left(s_1p_2\sqrt{\cos\theta+s_2\sin\theta}-s_2p_1\sqrt{\cos\theta+s_1\sin\theta}\right)\right]$$

$$v^I=K_I\sqrt{\frac{2r}{\pi}}\,\mathrm{Re}\left[\frac{1}{s_1-s_2}\left(s_1q_2\sqrt{\cos\theta+s_2\sin\theta}-s_2q_1\sqrt{\cos\theta+s_1\sin\theta}\right)\right] \tag{6}$$

$$w^I=0$$

$$\sigma_{xx}^{I} = \frac{K_I}{\sqrt{2\pi r}}\mathrm{Re}\left[\frac{s_1 s_2}{s_1 - s_2}\left(\frac{s_2}{\sqrt{\cos\theta + s_2 \sin\theta}} - \frac{s_1}{\sqrt{\cos\theta + s_1 \sin\theta}}\right)\right]$$

$$\sigma_{yy}^{I} = \frac{K_I}{\sqrt{2\pi r}}\mathrm{Re}\left[\frac{1}{s_1 - s_2}\left(\frac{s_1}{\sqrt{\cos\theta + s_2 \sin\theta}} - \frac{s_2}{\sqrt{\cos\theta + s_1 \sin\theta}}\right)\right] \tag{7}$$

$$\sigma_{xy}^{I} = \frac{K_I}{\sqrt{2\pi r}}\mathrm{Re}\left[\frac{s_1 s_2}{s_1 - s_2}\left(\frac{1}{\sqrt{\cos\theta + s_1 \sin\theta}} - \frac{1}{\sqrt{\cos\theta + s_2 \sin\theta}}\right)\right]$$

- Mode II

$$u^{II} = K_{II}\sqrt{\frac{2r}{\pi}}\mathrm{Re}\left[\frac{1}{s_1 - s_2}\left(p_2\sqrt{\cos\theta + s_2 \sin\theta} - p_1\sqrt{\cos\theta + s_1 \sin\theta}\right)\right]$$

$$v^{II} = K_{II}\sqrt{\frac{2r}{\pi}}\mathrm{Re}\left[\frac{1}{s_1 - s_2}\left(q_2\sqrt{\cos\theta + s_2 \sin\theta} - q_1\sqrt{\cos\theta + s_1 \sin\theta}\right)\right] \tag{8}$$

$$w^{II} = 0$$

$$\sigma_{xx}^{II} = \frac{K_{II}}{\sqrt{2\pi r}}\mathrm{Re}\left[\frac{1}{s_1 - s_2}\left(\frac{s_2^2}{\sqrt{\cos\theta + s_2 \sin\theta}} - \frac{s_1^2}{\sqrt{\cos\theta + s_1 \sin\theta}}\right)\right]$$

$$\sigma_{yy}^{II} = \frac{K_{II}}{\sqrt{2\pi r}}\mathrm{Re}\left[\frac{1}{s_1 - s_2}\left(\frac{1}{\sqrt{\cos\theta + s_2 \sin\theta}} - \frac{1}{\sqrt{\cos\theta + s_1 \sin\theta}}\right)\right] \tag{9}$$

$$\sigma_{xy}^{II} = \frac{K_{II}}{\sqrt{2\pi r}}\mathrm{Re}\left[\frac{1}{s_1 - s_2}\left(\frac{s_1}{\sqrt{\cos\theta + s_1 \sin\theta}} - \frac{s_2}{\sqrt{\cos\theta + s_2 \sin\theta}}\right)\right]$$

where Re denotes the real part of the statement and K_I and K_{II} are stress intensity factors for mode I and mode II, respectively. c_{ij} are compliance matrix components. p_i and q_i can be defined by

$$p_i = c_{11}s_i^2 + c_{12} - c_{16}s_i \quad i = 1,2 \tag{10}$$

$$q_i = c_{12}s_i + \frac{c_{22}}{s_i} - c_{26} \quad i = 1,2 \tag{11}$$

3. Crack-tip orthotropic enrichment functions

Crack-tip enrichment functions have been obtained in a way that include all possible displacement states in the vicinity of crack-tip, as described by in equations (6) and (8) [8]. These functions span the possible displacement space that may occur in the analytical solution. These are defined as [8]

$$\begin{aligned}\mathbf{Q}(r,\theta) &= \left[Q_1, Q_2, Q_3, Q_4\right] \\ &= \left[\sqrt{r}\cos\frac{\theta_1}{2}\sqrt{g_1(\theta)}, \sqrt{r}\cos\frac{\theta_2}{2}\sqrt{g_2(\theta)}, \sqrt{r}\sin\frac{\theta_1}{2}\sqrt{g_1(\theta)}, \sqrt{r}\sin\frac{\theta_2}{2}\sqrt{g_2(\theta)}\right]\end{aligned} \tag{12}$$

where

$$\theta_j = \arctan\left(\frac{s_{jy}\sin\theta}{\cos\theta + s_{jx}\sin\theta}\right) \tag{13}$$

$$g_j(\theta) = \sqrt{\left(\cos\theta + s_{jx}\sin\theta\right)^2 + \left(s_{jy}\sin\theta\right)^2} \tag{14}$$

with $j = 1,2$. In the above equations s_{jx} and s_{jy} are real and imaginary parts of s_j computed by equation (5), respectively.

Orthotropic enrichment functions mentioned in equation (12) are enrichment functions which are used in eXtended Finite Element Method (XFEM). The algorithm for applying these functions in the element free Galerkin method will be explained in the following sections.

4. EFG formulation

Consider a standard two-dimensional problem of linear elasticity in the domain Ω bounded by Γ, as shown in Figure 2. The equilibrium equation, natural and essential boundary conditions for such a problem can be written as

$$\mathbf{L}^T\boldsymbol{\sigma}+\mathbf{b}=0 \quad \text{in } \Omega \tag{15}$$

$$\boldsymbol{\sigma}\mathbf{n}=\bar{\mathbf{t}} \quad \text{on } \Gamma_t \tag{16}$$

$$\mathbf{u}=\bar{\mathbf{u}} \quad \text{on } \Gamma_u \tag{17}$$

where $\mathbf{L}$ is the differential operator defined as

$$\mathbf{L}=\begin{bmatrix} \dfrac{\partial}{\partial X_1} & 0 \\ 0 & \dfrac{\partial}{\partial X_2} \\ \dfrac{\partial}{\partial X_2} & \dfrac{\partial}{\partial X_1} \end{bmatrix} \tag{18}$$

and $\boldsymbol{\sigma}$, $\mathbf{u}$ and $\mathbf{b}$ are the stress, displacement and body force vectors, respectively. $\bar{\mathbf{t}}$ is the prescribed traction on the natural (traction) boundaries; $\bar{\boldsymbol{u}}$ is the prescribed displacement on the essential (displacement) boundaries and $\mathbf{n}$ is the vector of unit outward normal at a point on the natural boundary (see Figure 2).

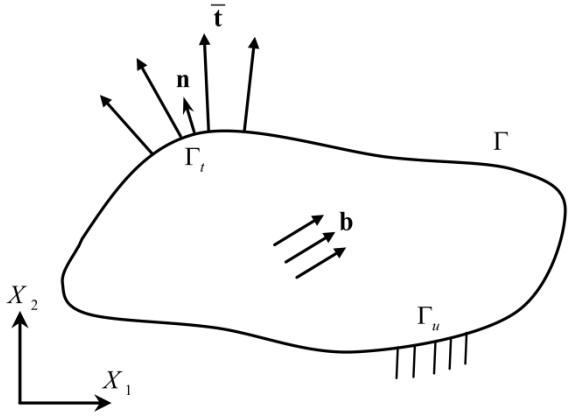

Figure 2. A two-dimensional continuum.

The standard un-constrained weak form of equation (15) is posed as

$$\int_\Omega \left(\mathbf{L}\delta\mathbf{u}\right)^{\mathrm{T}}\left(\mathbf{DLu}\right)\mathrm{d}\Omega-\int_\Omega \delta\mathbf{u}^{\mathrm{T}}\mathbf{b}\mathrm{d}\Omega-\int_{\Gamma_t}\delta\mathbf{u}^{\mathrm{T}}\bar{\mathbf{t}}\mathrm{d}\Omega=0 \tag{19}$$

where $\mathbf{D}$ is the matrix of elastic constants (inverse of compliance matrix $\boldsymbol{c}$ defined in equation (1)).

The problem domain is now represented by a set of field nodes for the purpose of field variable (displacement) approximation. These nodes are numbered sequentially from 1 to n for the entire problem domain. In EFG method, the Moving Least Squares (MLS) shape functions, presented in [11], are used to approximate the displacements at any point of interest using a set of nodes in the local support domain of the point. For using the enrichment functions of XFEM, the original displacement approximation (see [4]) changes to

$$\mathbf{u}^{\mathrm{h}}(\mathbf{X}) = \sum_{\mathrm{i}=1}^{\mathrm{n}} \varphi_{\mathrm{i}}(\mathbf{X}) u_{\mathrm{i}} + \sum_{\mathrm{k}=1}^{\mathrm{mt}} \varphi_{\mathrm{k}}(\mathbf{X}) \sum_{\alpha=1}^{4} \mathrm{Q}_{\alpha}(\mathbf{X}) b_{\mathrm{K}} \tag{20}$$

where $\varphi_{\mathrm{i}}(\mathbf{X})$ is the MLS shape function associated to node i, and $\boldsymbol{u}_i$ is the vector of regular nodal degrees of freedom. $\boldsymbol{b}_K$ is the vector of additional nodal degrees of freedom for modeling crack-tips, mt is the set of nodes that the discontinuity is in their influence (support) domain and $\mathrm{Q}_{\alpha}(\mathbf{X})$ is the enrichment function (e.g. functions defined in equation (12) for orthotropic materials).

In equation (20), $u^{\mathrm{h}}(\mathbf{X})$ is the approximated displacement of a point of interest $\mathbf{X}$. The first term in the right-hand side of equation (20) is the classical EFG approximation to determine the displacement field, while the second term is the enrichment approximation for enforcement of analytical solution near the crack-tip into the approximation (for increasing the accuracy of approximation near a crack-tip).

After manipulating equation (19) by equation (20), the final discretized system equations for the developed discontinuous enriched EFG has been derived as

$$\mathbf{KU} = \mathbf{F} \tag{21}$$

where $\mathbf{K}$ is the global stiffness matrix, $\mathbf{U}$ is the global displacement vector that collects the nodal displacements of all nodes in the entire problem domain and additional degrees of freedom produced by enrichments and $\mathbf{F}$ is the global force vector. $\mathbf{K}$ and $\mathbf{U}$ are assembled from the nodal stiffness matrix and the nodal force vector, respectively.

$$\mathbf{K}_{\mathrm{ij}}^{\mathrm{n}} = \begin{bmatrix} \mathbf{K}_{\mathrm{ij}}^{uu} & \mathbf{K}_{\mathrm{ij}}^{ub} \\ \mathbf{K}_{\mathrm{ij}}^{bu} & \mathbf{K}_{\mathrm{ij}}^{bb} \end{bmatrix} \tag{22}$$

$$\mathbf{F}_i^n = \begin{Bmatrix} \mathbf{F}_{\mathrm{i}}^{u} & \mathbf{F}_{\mathrm{i}}^{b_1} & \mathbf{F}_{\mathrm{i}}^{b_2} & \mathbf{F}_{\mathrm{i}}^{b_3} & \mathbf{F}_{\mathrm{i}}^{b_4} \end{Bmatrix}^{\mathrm{T}} \tag{23}$$

which

$$\mathbf{K}_{\mathrm{ij}}^{\mathrm{rs}} = \int_{\Omega} \left(\mathbf{B}_{\mathrm{i}}^{\mathrm{r}}\right)^{\mathrm{T}} \mathbf{D} \mathbf{B}_{\mathrm{j}}^{\mathrm{s}} \mathrm{d}\Omega \quad (\mathrm{r,s} = u, b) \tag{24}$$

$$\mathbf{F}_{\mathrm{i}}^{u} = \int_{\Omega} \mathbf{\Phi}_{\mathrm{i}}^{\mathrm{T}} \mathbf{b} \mathrm{d}\Omega + \int_{\Gamma_{\mathrm{t}}} \mathbf{\Phi}_{\mathrm{i}}^{\mathrm{T}} \bar{\mathbf{t}} \mathrm{d}\Gamma \tag{25}$$

$$\mathbf{F}_{\mathrm{i}}^{b_\alpha} = \int_{\Omega} \mathbf{\Phi}_{\mathrm{i}}^{\mathrm{T}} \mathrm{Q}_{\alpha} \mathbf{b} \mathrm{d}\Omega + \int_{\Gamma_{\mathrm{t}}} \mathbf{\Phi}_{\mathrm{i}}^{\mathrm{T}} \mathrm{Q}_{\alpha} \bar{\mathbf{t}} \mathrm{d}\Gamma \quad (\alpha = 1,2,3,4) \tag{26}$$

In the above equations, $\mathbf{\Phi}_{\mathrm{i}}(\mathbf{X})$ is the MLS shape function associated to node i, Q_α are enrichment functions defined in equation (12), $\mathbf{D}$ is the matrix of elastic constants, $\mathbf{B}_{\mathrm{i}}^{u}$ and $\mathbf{B}_{\mathrm{i}}^{b}$ are matrices of shape function derivatives,

$$\mathbf{B}_{\mathrm{i}}^{u} = \begin{bmatrix} \varphi_{\mathrm{i,x}} & 0 \\ 0 & \varphi_{\mathrm{i,y}} \\ \varphi_{\mathrm{i,y}} & \varphi_{\mathrm{i,x}} \end{bmatrix} \tag{27}$$

$$\mathbf{B}_{\mathrm{i}}^{b} = \begin{bmatrix} \mathbf{B}_{\mathrm{i}}^{b_1} & \mathbf{B}_{\mathrm{i}}^{b_2} & \mathbf{B}_{\mathrm{i}}^{b_3} & \mathbf{B}_{\mathrm{i}}^{b_4} \end{bmatrix} \tag{28}$$

$$\mathbf{B}_{\mathrm{i}}^{\alpha} = \begin{bmatrix} \left(\varphi_{\mathrm{i}} \mathrm{Q}_{\alpha}\right)_{,\mathrm{x}} & 0 \\ 0 & \left(\varphi_{\mathrm{i}} \mathrm{Q}_{\alpha}\right)_{,\mathrm{y}} \\ \left(\varphi_{\mathrm{i}} \mathrm{Q}_{\alpha}\right)_{,\mathrm{y}} & \left(\varphi_{\mathrm{i}} \mathrm{Q}_{\alpha}\right)_{,\mathrm{x}} \end{bmatrix} \quad (\alpha = 1,2,3,4) \tag{29}$$

In equation (21), $\mathbf{U}$ is in the form of

$$\mathbf{U} = \begin{Bmatrix} \mathbf{u} & \mathbf{b}_1 & \mathbf{b}_2 & \mathbf{b}_3 & \mathbf{b}_4 \end{Bmatrix}^{\mathrm{T}} \tag{30}$$

After solving equation (21) and obtaining $\mathbf{U}$, the nodal displacements $\mathbf{u}^{\mathrm{h}}(\mathbf{X})$ can be obtained by solving equation (20). Then, the strain and stress components can be retrieved using equations (31) and (32), respectively.

$$\boldsymbol{\varepsilon} = \mathbf{L}\mathbf{u}^{\mathrm{h}} \tag{31}$$

and

$$\boldsymbol{\sigma} = \mathbf{D}\boldsymbol{\varepsilon} \tag{32}$$

Since the MLS shape functions lack the Kronecker delta function property, it is necessary to apply a technique to enforce the essential (displacement) boundary conditions. In this study, the Lagrange multiplier method is adopted. The Lagrange multiplier method provides an efficacious way to implement essential boundary conditions and was used in the EFG method by Belytschko et al. [4].

The final discretized system equations for the proposed approach accompanied by the Lagrange multiplier method for enforcement of essential boundary conditions are changed to

$$\begin{bmatrix} \mathbf{K} & \mathbf{G} \\ \mathbf{G}^{\mathrm{T}} & 0 \end{bmatrix} \begin{Bmatrix} \mathbf{U} \\ \boldsymbol{\Lambda} \end{Bmatrix} = \begin{Bmatrix} \mathbf{F} \\ \mathbf{q} \end{Bmatrix} \tag{33}$$

$\mathbf{K}$, $\mathbf{U}$ and $\mathbf{F}$ have been defined in equation (21); $\boldsymbol{\Lambda}$ is a vector that collects the nodal Lagrange multipliers for all field nodes on essential boundaries; $\mathbf{G}$ is the global Lagrange matrix formed by assembling the nodal Lagrange matrix, $\mathbf{G}_{\mathrm{ij}}$, that is defined as

$$\mathbf{G}_{\mathrm{ij}}^{\mathrm{T}} = -\int_{\Gamma_{\mathrm{u}}} \mathbf{N}_{\mathrm{i}}^{\mathrm{T}} \boldsymbol{\Phi}_{\mathrm{j}} \mathrm{d}\Gamma - \int_{\Gamma_{\mathrm{u}}} \mathbf{N}_{\mathrm{i}}^{\mathrm{T}} \boldsymbol{\Phi}_{\mathrm{j}} \mathrm{Q}_{\alpha} \mathrm{d}\Gamma \qquad (\alpha = 1,2,3,4) \tag{34}$$

In equation (33), $\mathbf{q}$ is the global Lagrange vector formed by assembling the nodal Lagrange vector, $\mathbf{q}_{\mathrm{i}}$, defined in the following form

$$\mathbf{q}_{\mathrm{i}} = -\int_{\Gamma_{\mathrm{u}}} \mathbf{N}_{\mathrm{i}}^{\mathrm{T}} \bar{\mathbf{u}} \mathrm{d}\Gamma \tag{35}$$

In equations (34) and (35), the shape function $\mathbf{N}_i$ can be the Lagrange interpolants used in the conventional FEM. The first order Lagrange interpolant (the linear interpolation) which applied in this paper, can be given in the following form

$$N_1(z) = \frac{z - z_2}{z_1 - z_2}, \quad N_2(z) = \frac{z - z_1}{z_2 - z_1} \tag{36}$$

In a simple case, the essential boundaries are discretized using the line segments; The Lagrange multiplier at z is interpolated using two nodes at the two ends of this line segments.

5. Support domain selection near a crack

To represent discontinuity in a cracked problem, the following approach has been used in this paper. Since the definition of weight function in MLS depends on the distance between nodes, every change in selection of the support domain results in a change in weight functions.

The adopted approach way to select a support domain of radius r_s near the crack face is illustrated in Figure 3(a). It is noted that the nodes at the opposite side of the crack face are not considered. For nodes near a crack-tip, as depicted in Figure 3(b), to determine the distance of interest node $\mathbf{X}_i$ and arbitrary node $\mathbf{X} = (X_1, X_2)$ near a crack-tip, instead of considering the amount of $d_0(\mathbf{X})$, the amount of $d_1 + d_2(\mathbf{X})$ is considered where

$$d_0(\mathbf{X}) = \|\mathbf{X} - \mathbf{X}_i\|, \quad d_1 = \|\mathbf{X}_i - \mathbf{X}_C\|, \quad d_2(\mathbf{X}) = \|\mathbf{X} - \mathbf{X}_C\|$$

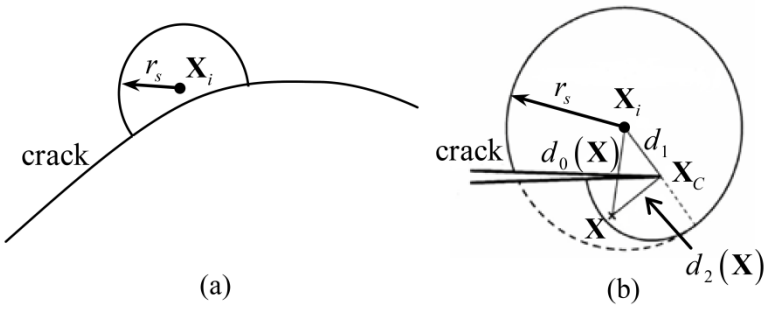

Figure 3. Selection of support domain near a crack: (a) crack face; (b) crack-tip.

6. Computation of stress intensity factors

The stress intensity factor (SIF) is one of the important parameters representing fracture properties of a crack. In this paper, stress intensity factors are evaluated to compare the accuracy of the developed EFG with other methods. In this study, the technique developed by Kim and Paulino [9] for computation of mixed-mode stress intensity factor, is employed and briefly reviewed.

The standard path independent J -integral for a crack is defined as [12]

$$J = \int_{\Gamma}\left[W_s\delta_{1j} - \sigma_{ij}\frac{\partial u_i}{\partial x_1}\right]n_j d\Gamma \tag{37}$$

where Γ is an arbitrary contour surrounding the crack-tip which encloses no other cracks or discontinuities, W_s is the strain energy density, $W_s = \frac{1}{2}\sigma_{ij}\varepsilon_{ij}$ for linear elastic material, n_j is the j th component of the outward unit normal to Γ, δ_{1j} is the Kronecker delta and the co-ordinates are taken to be the local crack-tip co-ordinates with the x_1-axis parallel to the crack face.

Now suppose there are two equilibrium states; state 1 corresponds to actual state that is obtained by analysis of the problem and state 2 corresponds to an auxiliary state for the given problem geometry. The auxiliary stress and displacement fields are defined by asymptotic fields near a crack-tip as given by analytical solutions (6), (7), (8) and (9).

By combining the actual and auxiliary solutions for obtaining the J-integral one can write:

$$J^{(act+aux)} = J^{(act)} + J^{(aux)} + M \tag{38}$$

where $J^{(act+aux)}$ is the J-integral value for the superposition state, $J^{(act)}$ and $J^{(aux)}$ are the J-integral value for actual and auxiliary states, respectively, and

$$M = \int_{\Gamma}\left[W^M\delta_{1j} - \sigma_{ij}\frac{\partial u_i^{aux}}{\partial x_1} - \sigma_{ij}^{aux}\frac{\partial u_i}{\partial x_1}\right]n_j d\Gamma \tag{39}$$

where W^M is strain energy density that is defined as follow for linear-elastic conditions

$$W^M = \frac{1}{2}\left(\sigma_{ij}\varepsilon_{ij}^{aux} + \sigma_{ij}^{aux}\varepsilon_{ij}\right) \tag{40}$$

The strain of auxiliary field is defined as

$$\varepsilon_{ij}^{aux} = \frac{1}{2}\left(u_{i,j}^{aux} + u_{j,i}^{aux}\right) \tag{41}$$

After some manipulations, M can be written in the form of [8]

$$M = 2e_{11}K_I K_I^{aux} + e_{12}\left(K_I K_{II}^{aux} + K_I^{aux} K_{II}\right) + 2e_{22}K_{II}K_{II}^{aux} \tag{42}$$

where

$$e_{11} = -\frac{c_{22}}{2}\,\mathrm{Im}\left(\frac{s_1+s_2}{s_1 s_2}\right) \tag{43}$$

$$e_{12} = -\frac{c_{22}}{2}\,\mathrm{Im}\left(\frac{1}{s_1 s_2}\right) + \frac{c_{11}}{2}\,\mathrm{Im}(s_1 s_2) \tag{44}$$

$$e_{22} = \frac{c_{11}}{2}\,\mathrm{Im}(s_1+s_2) \tag{45}$$

In the above equations, c_{ij} is the compliance matrix component and s_1, s_2 are the roots of equation (5).

The SIFs for the problem can be obtained by considering the two states (state I: $K_I^{aux}=1$, $K_{II}^{aux}=0$; state II: $K_I^{aux}=0$, $K_{II}^{aux}=1$) and solving a system of linear algebraic equations:

$$\begin{aligned} M^{(act,stateI)} &= 2e_{11}K_I + e_{12}K_{II} \\ M^{(act,stateII)} &= e_{12}K_I + 2e_{22}K_{II} \end{aligned} \tag{46}$$

In order to solve the system of equations, M must be calculated from equation (39) and then compared with equation (46).

7. Numerical simulations

7.1. A rectangular plate with an edge crack under uniaxial tensile distributed load

In this example, the proposed method is applied to an edge horizontal crack in a rectangular plate subjected to tensile distributed load. The plate is considered in the plane stress state and several orientations of material elastic axes are studied. The proportions of width to height and crack length to width are equal to 0.5 (see Figure 4). The plate is composed of a graphic-epoxy material with orthotropic properties as:

$$E_1 = 11.71\times10^5 \ \frac{\mathrm{kg}}{\mathrm{cm}^2} \ (114.8 \ \mathrm{Gpa}), \qquad E_2 = 1.19\times10^5 \ \frac{\mathrm{kg}}{\mathrm{cm}^2} \ (11.7 \ \mathrm{Gpa})$$

$$G_{12} = 9.85\times10^4 \ \frac{\mathrm{kg}}{\mathrm{cm}^2} \ (9.66 \ \mathrm{Gpa}), \qquad \nu_{12} = 0.21$$

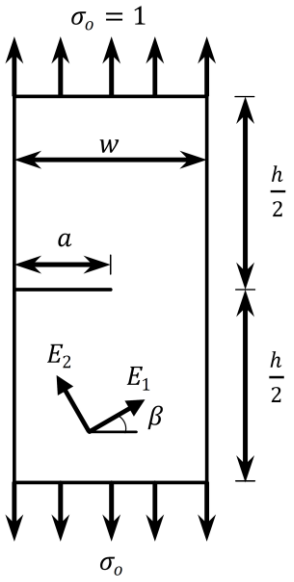

Figure 4. Geometry and loading of the rectangular plate with an edge crack.

The EFG model is composed of 1984 field nodes (Figure 5a) and 1891 background cells for integration. The enriched nodes are shown in Figure 5b. 48 degrees of freedom are added to usual EFG degrees of freedom for enrichment. The proportion of support domain

dimension to nodal spacing is considered 1.7. The mixed mode stress intensity factors are calculated as described with the relative integration domain size of about 0.16 of crack length. Effects of changing the material elastic angle on mixed mode stress intensity factors in the plate are probed. The comparison of results between the proposed method and the results by Asadpoure et al. [8] who performed similar studies using the extended finite element method, is shown in Figure 6.

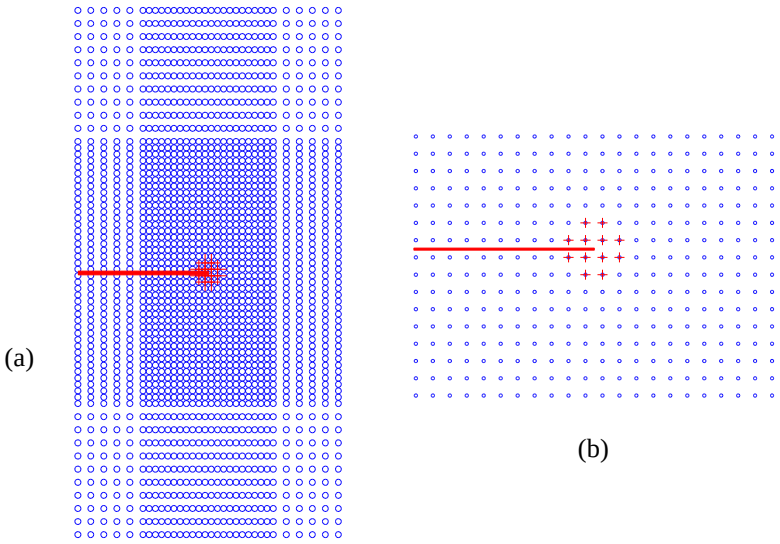

Figure 5. Nodal distribution for the rectangular plate with an edge crack: (a) whole view of EFG model; (b) enlarged view of nodal distribution around the crack-tip (enriched nodes are distinguished by red cross signs).

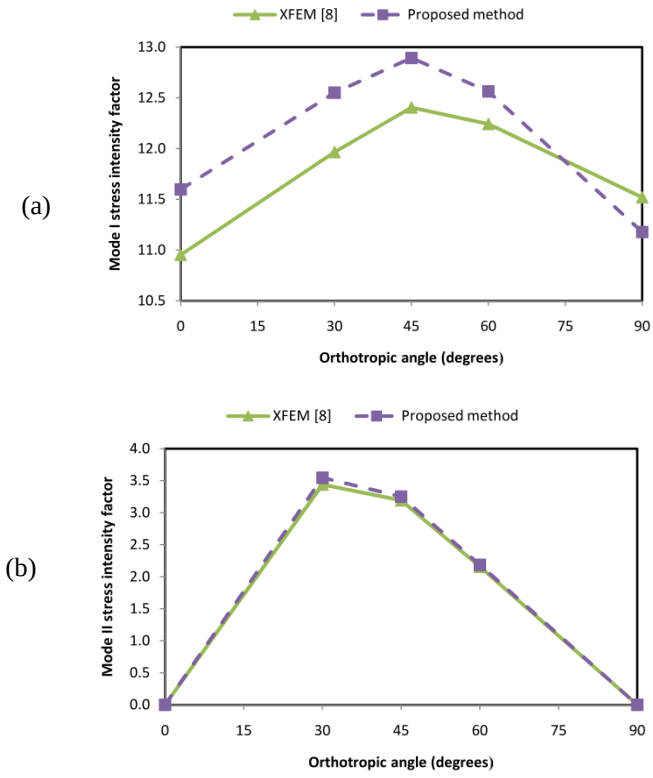

Figure 6. The effect of various inclinations of elastic material axes on the stress intensity factors: (a) mode I stress intensity factor; (b) mode II stress intensity factor.

The results show that the trend of mode I stress intensity factor changes around $\beta = 45°$. It has an increasing trend in the span of $\beta = 0°$ to $\beta = 45°$ and then decreases in the span of $\beta = 45°$ to $\beta = 90°$ and reaches a value around its initial value, i.e. when $\beta = 0°$. The turning point for the mode II stress intensity factor is about $\beta = 30°$.

Table 1 shows the s values computed by equation (5) for different angles of elastic material axes with respect to the horizontal line (β).

Table 1. s values for different β.

β	s_1	$\bar{s}_1$	s_2	$\bar{s}_2$
0	0 + 0.9652i	0 - 0.9652i	0 + 3.2454i	0 - 3.2454i
30	0.0301 + 0.9820i	0.0301 - 0.9820i	-1.2201 + 0.9593i	-1.2201 - 0.9593i
45	0.0354 + 0.9994i	0.0354 - 0.9994i	-0.8266 + 0.5628i	-0.8266 - 0.5628i
60	0.0312 + 1.0174i	0.0312 - 1.0174i	-0.5065 + 0.3982i	-0.5065 - 0.3982i
90	0 + 1.0361i	0 - 1.0361i	0 + 0.3081i	0 - 0.3081i

7.2. A central crack in a square plate subjected to tension

The next problem considered is shown in Figure 7. It consists of a finite orthotropic body containing a central crack and subjected to tension. The material and crack axes coincide. This problem was solved by Bowie and Freese [13] by the boundary collocation method for a variety of material properties and geometric ratios. Conditions of plane stress were assumed.

The geometric parameters are chosen here to be $h/w = 1$ and $a/w = 0.3$. The material properties: E_2, G_{12} and ν_{12} are the same as the previous example but E_1 is considered $(0.5, 1.5, 2.5, 4.5) \times E_2$. These sets of parameters are chosen to examine the effect of the ratio E_1/E_2 on solution accuracy.

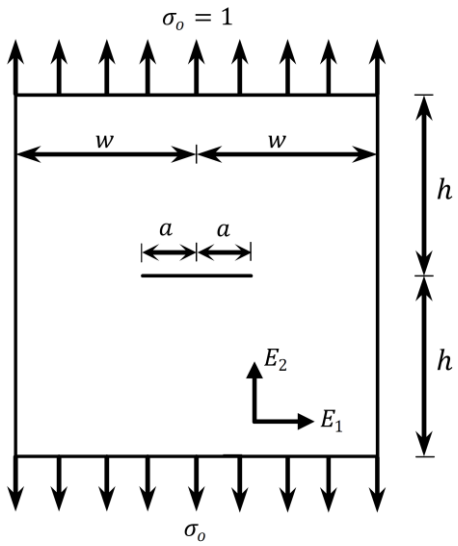

Figure 7. Finite orthotropic body containing a central crack.

As shown in Figure 8, 7344 field nodes and 7171 background cells are used for modeling and integration, respectively. Results for the normalized stress intensity factors $\left(K_I/\sigma_o\sqrt{\pi a}\right)$ are shown in Table 2, together with those obtained by Bowie and Freese [13]. The present results show good agreement, with an average difference of 0.99 percent.

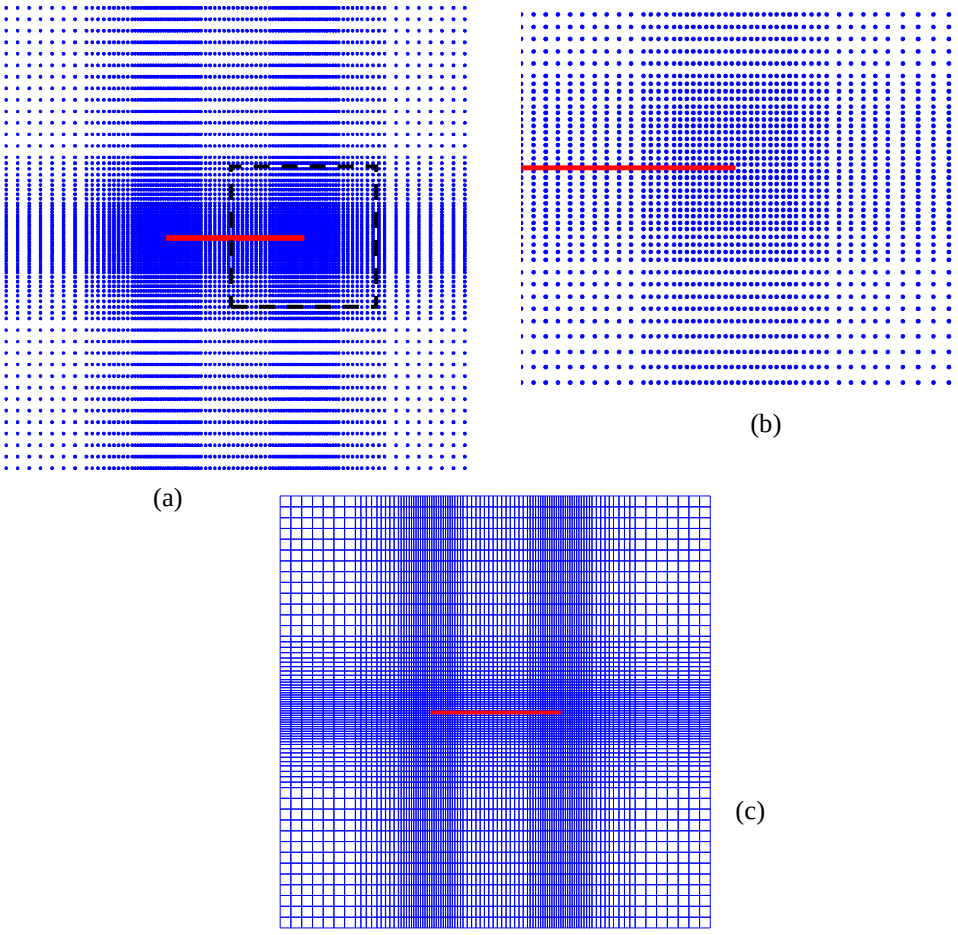

Figure 8. Discretization of the square plate with a central crack: (a) nodal distribution in entire domain; (b) nodal distribution around the crack-tip; (c) background cells.

Table 2. Normalized mode I SIF $\bar{K}_I = K_I/\sigma_o\sqrt{\pi a}$ for different sets of material parameters.

E_1/E_2	$\bar{K}_I$		Difference (%)
	Proposed approach	Bowie and Freese [13]	
0.5	1.1427	1.17	2.33
1.5	1.1019	1.10	0.17
2.5	1.0885	1.08	0.79
4.5	1.0773	1.07	0.68

8. Conclusions

In this contribution, the conventional EFG has been further extended to analysis of cracked orthotropic plates. The newly developed crack-tip orthotropic enrichment functions have been employed in the EFG method to increase the approximation accuracy near the crack-tip. Moreover, by using an appropriate way of support domain selection near the crack, the discontinuity has been modeled without defining any further enrichment functions. Also, for imposition of essential boundary conditions, the Lagrange multiplier method has been utilized and its formulations have been modified according to the enrichment functions.

Some numerical examples have been analyzed using the proposed approach. Results of mixed-mode stress intensity factors (SIFs) have been compared with the reference results and proved the accuracy, robustness and efficiency of the proposed orthotropic enriched EFG.

References

[1] N.I. Muskelishvili, *Some Basic Problems on the Mathematical Theory of Elasticity*, Noordhoof, Groningen, 1952.

[2] G.C. Sih, P.C. Paris, G.R. Irwin, On cracks in rectilinearly anisotropic bodies, *Int. J. Fract. Mech.*, Vol. 1, (1965) 189–203.

[3] L. Nobile, C. Carloni, Fracture analysis for orthotropic cracked plates, *Compos. Struct.*, Vol. 68, 3 (2005) 285–293.

[4] T. Belytschko, Y.Y. Lu, L. Gu, Element-free Galerkin methods, *Int. J. Numer. Meth. Eng.*, Vol. 37, (1994) 229–256.

[5] S. Mohammadi, *Extended Finite Element Method for Fracture Analysis of Structures*, Blackwell/Wiley Press (UK), 2008.

[6] A. Asadpoure, S. Mohammadi, A. Vafai, Modeling crack in orthotropic media using a coupled finite element and partition of unity methods, *Finite Elements Anal. Des.*, Vol. 42, 13 (2006), 1165-1175.

[7] A. Asadpoure, S. Mohammadi, A. Vafai, Crack analysis in orthotropic media using the extended finite element method, *Thin Walled Struct.*, Vol. 44, 9 (2006) 1031-1038.

[8] A. Asadpoure, S. Mohammadi, Developing new enrichment functions for crack simulation in orthotropic media by the extended finite element method, *International Journal for Numerical Methods in Engineering*, Vol. 69, 10 (2007) 2150–2172.

[9] J.H. Kim, G.H. Paulino, The interaction integral for fracture of orthotropic functionally graded materials: evaluation of stress intensity factors, *Int. J. Solids Struct.*, Vol. 40, (2003) 3967–4001.

[10] S.G. Lekhnitskii, *Theory of an Anisotropic Elastic Body*, Holden-Day, San Francisco, 1963.

[11] P. Lancaster, K. Salkauskas, Surfaces generated by moving least squares methods, *Math. Comput*., Vol. 37, (1981) 141-158.

[12] J.R. Rice, Path-independent integral and the approximate analysis of strain concentration by notches and cracks, *Journal of Applied Mechanics*, Transactions (ASME), Vol. 35, 2 (1968) 379–386.

[13] O.L. Bowie, C.E. Freese, Central crack in plane orthotropic rectangular sheet, *Int. J. Fract. Mech.*, Vol. 8, 1 (1972) 49-58.